RSC Advances

ROYAL SOCIETY OF CHEMISTRY

www.rsc.org/advances

Influence of interface combination of reduced graphene oxide/P25 composites on their visible photocatalytic performance

Yueli Liu, Keqiang Chen, Mengyun Xiong, Peng Zhou, Zhuoyin Peng, Guojie Yang, Yuqing Cheng, Ruibing Wang, Wen Chen*

* To whom correspondence should be addressed:

[*] State Key Laboratory of Advanced Technology for Materials Synthesis and Processing, and School of Materials Science and Engineering, Wuhan University of Technology, Wuhan, 430070 (P. R. China)

Correspondent:

[*] Prof. W. Chen

Tel.: +86-27-8765-1107

Fax: +86-27-8776-0129

E-mail: chenw@whut.edu.cn **(Wen Chen)**

Abstract

Reduced graphene oxide (RGO)/P25 composites are successfully synthesized by using a facile hydrothermal method, and Raman mapping images show that the P25 are very uniformly dispersed in the composite. The RGO/P25 composites are used as the photocatalysis towards methyl orange under UV and visible light illumination, respectively. The degradation ratio of 0.75 wt% RGO/P25 composite is the best one of 100% after 120 and 150 minutes' irradiation under the UV and visible light irradiation, respectively, which is greatly enhanced compared with that of the P25, especially in the visible light region. It is found that the good interface combination between RGO and P25 may improve the electric conductivity and life-time of photo-induced electrons in photodegradation process as well as the enhanced light absorption, which may favor for the efficiently enhancement of photodegradation rate of the RGO/P25 composite.

Keywords: Reduced graphene oxide (RGO)/P25 composites; hydrothermal method; photocatalytic performance; interface combination; Raman mapping image

1. Introduction

Photocatalytic performance of TiO_2 nanomaterials has attracted a lot of attentions since it is discovered by Fujishima in 1971. Currently many semiconductor photocatalysis has been

paid more attention to solve the environmental pollution, and how to make full use of the light energy is the key factor for the efficient and mild route to photodegrade the wastes, [1-8] and many efforts have been paid to promote its property by designing and modifying various TiO_2-based composites.

Among them, graphene-TiO_2 hybrid nanomaterials have been widely researched for its perfect property of graphene. High-reactive crystal facets and high dispersities of TiO_2 nanocrystals are synthesized on graphene surface by hydrothermal process. [9-10] It is also reported the graphene between the semiconductors can lengthen the life-time of photoexcited charge carriers in the semiconductor and then improve the photoactivity. [11-12] Many kinds of methods have been proposed to prepare the graphene/TiO_2 hybrid composites in photocatalysis. For example, Reduced graphene oxide (RGO) was applied to prepare various composites of RGO/photocatalyst of RGO/TiO_2, RGO/ZnO and RGO/Ta_2O_5, and the photocatalytic activities of the composites under UV and visible light were studied in degradation of methylene blue. [13] Electro-spinning method was used for the fabrication of one-dimensional TiO_2/graphene composites, which were used in the photodegradation of methyl orange. [14] TiO_2 nanoparticles on the surface of few layered graphene sheets were prepared by using a single step hydrothermal method, and their photocatalytic degradation ability under visible light were also studied. [15]

Normally, the interface combination between the graphene and TiO_2 nanomaterials is quite important for the understanding of the enhancement of their photocatalytic performance. [16-18] How to investigate the interface combination of the graphene-TiO_2 composites is quite important to reveal the influence of the resultant quality and structural properties of the composites on their photocatalytic performance. [19-20]

In the present work, we synthesize the reduced graphene oxide (RGO)/P25 composites by using a facile hydrothermal method, and use them in the photodegrade the methyl orange under UV and visible light irradiations, respectively. The influence of the interface combination of the composites on the photocatalytic performance is also studied.

2. Experimental

2.1 Synthesis of the RGO/P25 composites

Graphene oxide (GO) was prepared by Hummers method. [40] Firstly, 2 g graphite powders and 1.5 g $NaNO_3$ were mixed in an ice bath, and then put into the concentrated H_2SO_4 solution (80 mL). With vigorous stirring, 10 g $KMnO_4$ was gradually added and the temperature was kept below 20 ºC. Then, the mixture was stirred at 35 ºC in a water bath for 3 h. After reaction, the mixture became pasty with a brownish color. 100 mL H_2O was slowly added to the pasty mixture with putting the mixture in an ice bath to keep the temperature below 35 ºC. 10 mL of 30% H_2O_2 solvent was added to the mixture, and the color of this solution became a brilliant yellow. Then, the mixture was washed with 10% HCl (aq.) and deionized water in order. Finally, the resulting sample was dried under vacuum condition. GO with different weights was dissolved in 60 mL glycol solution, and sonicated for 2 h until the solution became clear, and then 3 g P25 powders were added into the solution. After vigorous stirring, the suspension was transferred into a Teflon-lined stainless steel autoclave (100 mL), and reacted at 180 ºC for 6 h. Finally, the products were filtered with distilled water and dried in a vacuum drier.

2.2 Photocatalytic activity experiments

Before the irradiation, 0.05g graphene-TiO_2 composites were put into aqueous methyl

orange solution (50 mL, 32.73 ppm), and then the suspension is stirred for 2 h in the dark environment to achieve the establishment of an adsorption/desorption equilibrium. Photogradation rate of graphene-TiO_2 composites was evaluated by examining the concentration variation of methyl orange under UV and visible light illumination from the light source of 125 W high-pressure Hg lamps for every 60 min, respectively, which has UV (200-400 nm) and visible light (400-800 nm) spectra with the main peak located at the 365 nm wavelength. For the visible light irradiation, the light source is equipped with an UV cutoff filter, which may remove 99% of UV light with the wavelength between 320 nm and 400 nm. The irradiation light intensity on the samples under UV and visible light illumination was kept equally by adjusting the distance between the lamp and samples.

2.3 Measurements

The crystal structure and microstructure of the samples were characterized by using X-ray diffraction (XRD, PertPro, PANalytical, Netherlands), Fourier transform infrared spectroscopy (FTIR) (TENSOR27, Bruker, Germany) and scanning electron microscope (FESEM, JSEM-5610LV, Japan). 3D Raman mapping image was measured by Confocal Raman System (WITec alpha300R, Germany) equipped with a 532 nm laser and optical diffraction limit of ~ 200 nm, the composite films were detected to obtain 3D information from the area of 100 μm×100 μm with a mesh of 2 μm at the center of graphene-TiO_2 composite films. UV-Vis absorption spectra (UV-2550, Shimadzu, Japan) were used to characterize the absorption properties of samples. The photoluminescence decay was measured using time-resolved fluorescence spectroscopy (HORIBA Fluoromax-4, France).

3. Results and Discussion

XRD patterns of the composites in Fig. 1(a) show that the diffraction peaks are originated from the anatase and rutile TiO_2 phases, and also identify that the relative content of anatase phase and rutile phase is about 4:1, which is accord well with the P25 peaks. Meanwhile, after decorated with RGO, there is no obvious peak changing at the various contents of the RGO/P25 composites if comparing with that of the P25, which is related to the fact that the RGO content is too little to be detected by XRD observation. However, there is a broadened peak in the range of 20-30 degree for the various RGO/P25 composites. Fig. 1(b) shows the section SEM image of 0.75 wt% RGO-P25 composites, which shows that the TiO_2 nanoparticles form some clusters on the surface of the RGO. It also shows that the other various RGO-P25 composites have the similar morphologies shown in Fig. S1.

Fig. 1(c) shows the FTIR spectra of the P25 and as-prepared RGO/P25 (0.75 wt %). For P25, the absorption peaks at 3612 cm^{-1} and 1621 cm^{-1} come from the –OH stretching group, while the small peaks at 400-900 cm^{-1} originate from the stretching vibration of Ti-O-Ti bonds in crystalline TiO_2. [21-22] Compared with that of the P25, the existed broad peaks around 1100 cm^{-1} originate from the stretching vibrations of C-O-C (1127 cm^{-1}) and C-OH (1048 cm^{-1}) bonds, which is caused by the partial existence of graphene oxide, as it is impossible to be totally reduced in the process. [23] However, for the RGO/P25 composites, the broad absorption below 1000 cm^{-1} is much plumper with a sharp peak than the corresponding peak in pure P25, which is attributed to be the presence of Ti-O-Ti vibration and Ti-O-C vibration (815 cm^{-1}). [23-24] Moreover, it is clear that the FTIR spectrum of the RGO/P25 composite shows some strong absorption peaks that correspond to some functional groups, such as CH_2 group (2925 cm^{-1}) and alcoholic C-OH stretching (1442 cm^{-1}).

As the interface combination of the graphene-TiO_2 composites is quite important for their

photocatalytic performance. Till now, many kinds of the microscopes have been used for evaluating the morphology and microstructure of the graphene hybrid film, such as high resolution transmission electron microscopy (HRTEM), [25-26] scanning probe microscopy (SPM), [27] atomic resolution scanning tunneling microscopy (STM), [28-29] low-energy electron microscopy (LEEM) [30-31] and so on, while that requires cumbersome sample preparation and a high level of technical expertise, and they cannot give a macroscopic image of the graphene distribution. Raman mapping image from Raman spectroscopy arises as a fast and useful tool for the distribution characterization of the composites containing carbon nanostructures, [16-18] as Raman spectra of TiO_2 and graphene show non-overlapping well-defined features, which provides the valuable distribution information of both components that can help to build a complete description of RGO/P25 composites.

Fig. 2(a) shows that the RGO and P25 are uniformly dispersed in the formed composites. Fig. 2(b) shows the Raman spectrum obtained by the zone in Fig. 2(a), and the characteristic peaks at 148 cm^{-1} ($E_{g(1)}$), 391 cm^{-1} (B_{1g}), 516 cm^{-1} (A_{1g}) and 637 cm^{-1} ($E_{g(2)}$) reveal that the existence of TiO_2. [33] The bands located at 1352, 1614 and 2671 cm^{-1} correspond to the D (breathing mode of A_{1g} symmetry), G (E_{2g} symmetry, in-plane bond-stretching motion of pairs of sp^2 C atoms) and 2D bands, respectively, which are the typical two bonds of the graphitic materials. The G band is a typical zone center vibration mode of graphite crystalline, corresponding to order sp^2 bonded carbon, whereas the D band is an edge vibration mode or disorder layer. The sharp peaks and narrow full width at half maximum of the G and D bands indicate a high graphitization degree of the carbon coating layer. [34]

The Raman data are reorganized into intensity mapping, and Fig. 2(c) and 2(d) show the Raman mapping image of RGO/P25 composites. Fig. 2(c) shows the image obtained from the

2D bands of the graphene. The 'bright' regions with high intensity show the existence of the graphene, while the 'dark' regions are related with the P25 information, which proves the uniform distribution of the graphene in the composites. The strongest band of anatase TiO_2 (E_g mode around 148 cm^{-1}) is selected as the P25 fingerprint, and the Raman mapping in Fig. 2(d) also shows that the P25 are quite uniformly dispersed in the composites. The Raman mapping image of 2D bands of the graphene in the other various RGO-P25 composites also prove it, as shown in Fig. S1. For comparison, the RGO-P25 composite is also prepared by mechanical mixing of the graphene and P25 together, and the corresponding SEM image and Raman mapping image are also shown Fig. S3. It is found that the graphene exists in cluster in the composite without good dispersion. Therefore, the RGO may be fairly homogeneously formed in the composites by the facile hydrothermal process.

UV-Vis spectra are used to character the optical absorption of all of the above samples in the wavelength range of 300-800 nm as shown in Fig. 3. It shows that the absorption edge of the RGO/P25 composites has no obvious peak-shifting, and it proves that there is no influence on the band gap of the P25 after the formation of the composites. Moreover, the RGO/P25 composites possess an obvious enhanced UV and visible light absorption comparing with P25, and the 0.75 wt% RGO/P25 composite has the highest optical absorption intensity. In addition, the well-combined RGO with P25 in the composites also favor for the rapid transferring of the photo-generated electrons and reduce the recombination of the photo-generated electrons and holes in the RGO/P25 composites.

The photocatalytic efficiency of the various RGO/P25 composites is evaluated in terms of the degradation rate of methylene orange (MO) under UV light and visible light irradiation, respectively. The ratio of the intensity of the MO's absorption bands before and after

irradiation (I/I_0) is correlated with irradiation time in Fig. 4 by choosing the absorption peak at 586 nm. It shows that the photodegradation rates may be enhanced both under the irradiation of UV and visible light after the formation of the RGO/P25 composite. For example, the photodegradation rate of the pure P25 are about 60.2% after 120 minutes' UV light irradiation, and that of 0.75 wt% RGO/P25 composite has the best photodegradation efficiency and may totally photodegrade the MO molecules as shown in Fig. 4(a).

Pure P25 almost has no photodegradation effect towards MO under visible light irradiation, while 0.75 wt% RGO/P25 composite has the best photodegradation efficiency and may totally photodegrade the MO molecules after 150 minutes' visible light irradiation as shown in Fig. 4(b). It shows that the reaction rate increases by a factor of 1.67 under UV-light irradiation and even a factor of hundreds under visible-light irradiation compared with that of the pure P25, which is quite good comparing with the others' similar reports. [13-15] Therefore, the RGO existed inside the P25 nanoparticles can efficiently enhance the photodegradation ability, which results from the fact that the graphene may accelerate the separation of photogenerated electrons and hole on P25 nanocrystals in the composites. [35] On the other hand, the excess content of graphene (1.00 wt%) will decrease the optical absorption due to the shading effect, [5, 36] and then decreases the photocatalytic properties, and it is in consistent with UV-Vis spectra in Fig. 3.

It is well known that a typical Schottky junction barrier at the interface between graphene and P25 will be formed, [37-38] as the heterojunctions will suppress the recombination of electron-hole pairs in P25 nanoparticles, where the RGO serves as an efficient electron traps aiding electron-hole separation. The possible mechanism of the RGO/P25 composites can be understood through their schematic diagram as shown in Fig. 5. In UV region, both of P25

and RGO are photoactive components in the composites, which can generate electrons and holes under illumination from the valence band (VB) to the conduction band (CB), which may migrate to the surface of the composites. The Schottky junction barrier facilitates the electron capture, and it will increase the life-time of the photo-excited electron-hole pairs and retards the electron-hole recombination to enhance the photocatalytic performance. Then the photo-excited electrons migrate to O_2 molecules adsorbed on the surface of P25 nanocrystals, [39-40] and subsequently reduce the recombination between electrons and holes, allowing more opportunities for the electrons to participate in the reduction reaction to form superoxide radicals (O_2^-), which serves as a strong oxidant that can decompose MO molecules effectively. The holes generated under irradiation on P25 participate in the oxidation reaction and then produce hydroxyl radicals (·OH), which is a very strong oxidant to favor for the decomposition of organic substances in parallel. Meanwhile, in visible light region, most of the photo-excited electrons are generated due to the RGO, [41-42] which may diffuse through the RGO/P25 interface into CB of P25, and the well-combined interface between the RGO and P25 may favor for the migration of the photo-excited electrons and then acceleration of the production of superoxide and hydroxyl radicals.

4. Conclusions

Various RGO/P25 composites with the well-combined interface are synthesized by using the hydrothermal method, and it is found that the RGO/P25 composites have an obvious enhanced photodegradation towards the methylene orange molecules, and the 0.75 wt% RGO/P25 composite possesses the best one with the total photodegradation after 120 and 150 minutes' irradiation under the UV and visible light irradiation, respectively. The good

interface combination between RGO and P25 may improve the electric conductivity and life-time of photo-induced electrons in photodegradation process as well as the enhanced light absorption, and it cause the enhancement of photodegradation rate of the RGO/P25 composites.

Acknowledgements

This work is supported by the International S&T Cooperation Program of China (ISTCP) ((No. 2013DFR50710) and Equipment pre-research project (No. 625010402).

References

[1] J. Zhang, J. H. Xi and Z. G. Ji, *J. Mater. Chem.,* 2012, **22**, 17700.

[2] Y. L. Liu, W. Shu, K. Q. Chen, Z. Y. Peng and W. Chen, *ACS Catal.,* 2012, **2**, 2557.

[3] J. Zhang, Y. P. Zhang, Y. K. Lei and C. X. Pan, *Catal. Sci. Technol.,* 2011, **1**, 273.

[4] Z. W. Zheng, C. J. Zhao, S. B Lu, Y. Chen, Y. Li, H. Zhang and S. C. Wen, *Opt. Express,* 2012, **20**, 23201.

[5] Y. L. Liu, W. Shu, Z. Y. Peng, K. Q. Chen and W. Chen, *Catal. Today,* 2013, **208**, 28.

[6] Y. L. Liu, L. Zhong, Z. Y. Peng, Y. Cai, Y. H. Song and W. Chen, *CrystEngComm,* 2011, **13**, 5467.

[7] H. J. Yan , H. X. Yang, *J. Alloys Comp.*, 2011, **509**, L26.

[8] Y. M. He, L. H. Zhang, X. X. Wang, Y. Wu, H. J. Lin, L. H. Zhao, W. Z. Weng, H. L. Wan, M. H. Fan, *RSC Adv.*, 2014, **4**, 13610.

[9] Q. L. Bao, H. Zhang, B. Wang, Z. H. Ni, C. Haley, Y. X. Lim, D. Y. Tang and K. P. Loh, *Nature Photonics,* 2011, **5**, 411.

[10]H. Zhang, S. Virally, Q. L. Bao, K. P. Loh, S. Massar, N. Godbout and P. Kockaert, *Opt. Lett.,* 2012, **37**, 1856.

[11]H. Tang, G. J. Ehlert and Y. Lin, *Nano Lett.,* 2011, **12**, 84.

[12]H. Zhang, D. Y. Tang, L. M. Zhao, Q. L. Bao and K. P. Loh, *Appl. Phys. Lett.,* 2010, **96**, 111112.

[13]H. Q. Sun, S. Z. Liu, S. M. Liu and S. B. Wang*, Appl. Catal. B-Environ.,* 2013, **146**, 162.

[14]P. N. Zhu, A. S. Nair and S. J. Peng, *ACS Appl. Mater. Interf.,* 2012, **4**, 581.

[15]G. S.Anjusree, A. S. Nair, S. V. Nair and S. Vadukumpully, *RSC Adv.,* 2013, **3**, 12933.

[16]S. Y. Treschev, P. W. Chou, Y. H. Tseng, J. B. Wang, E. V. Perevedentseva and C. L. Cheng, *Appl. Catal. B-Environ.,* 2008, **79**, 8.

[17]J. Lu, M. Y. Wang, Y. Li and C. H. Deng, *Nanoscale,* 2012, **4**, 1577.

[18]D. Graf, F. Molitor, K. Ensslin, C. Stampfer, A. Jungen, C. Hierold and L. Wirtz, *Eur. Phys. J. Special Topics,* 2007, **148**, 171.

[19] Y. L. Liu, Y. Q. Cheng, W. Shu, Z. Y. Peng, K. Q. Chen, J. Zhou, W. Chen and G. S. Zakharova, *Nanoscale,* 2014, **6**, 6755.

[20] W. Shu, Y. L. Liu, Z. Y. Peng, K. Q. Chen and W. Chen, *J. Alloy. Comp.,* 2013, **563**, 229.

[21] J. Zhang, W. Fu, J. H. Xi, H. He, S. C. Zhao, H. W. Lu and Z. G. Ji, *J. Alloys Comp.* 2013, *575*, 40–47.

[22] Y. L. Liu, G. J. Yang, H. Zhang, Y. Q. Cheng, K. Q. Chen, Z. Y. Peng and W. Chen, *RSC Advances* 2012, **4**, 24363.

[23] T. Szab, O. Berkesi, P. Forg, K. Josepovits, Y. Sanakis, D. Petridis and I. Dekany, *Chem. Mater.*, 2006, **18(11)**, 27402749.

[24] Z. Y. Peng, Y. L. Liu, W. Shu, K. Q. Chen and W. Chen, *Eur. J. Inorg. Chem.,* 2012, **32**, 5239.

[25] Ç. Ö. Girit, J. C. Meyer, R. Erni, M. D. Rossell, C. Kisielowski, L. Yang, C. H. Park, M. F. Crommie, M. L. Cohen, S. G. Louie and A. Zettl, *Science,* 2009, **323**, 1705.

[26] B. Krauss, P. Nemes-Incze, V. Skakalova, L. P. Biro, K. V. Klitzing and J. H. Smet, *Nano Lett.,* 2010, **10**, 4544.

[27] M. Ghislandi, G. G. Hoffmann, E. Tkalya, L. J. Xue and G. D. With, *Appl. Spectrosc. Rev.,* 2012, **47**, 371.

[28] L. Tapasztó, G. Dobrik, P. Lambin and L. P. Biró, *Nature Nanotechnol.,* 2008, **3**, 397.

[29] H. Hibino, H. Kageshima, F. Maeda, M. Nagase, Y. Kobayashi and H. Yamaguchi, *Phys. Rev. B,* 2008, **77**, 075413.

[30] H. Hibino, S. Mizuno, H. Kageshima, M. Nagase and H. Yamaguchi*, Phys. Rev. B,* 2009, **80**, 085406.

[31] M. Nagase, H. Hibino, H. Kageshima and H. Yamaguchi, *Nanotech. ,* 2009, **20**, 445704.

[32] Z. Y. Peng, Y. L. Liu, W. Shu, K. Q. Chen and W. Chen, *Chem. Eng. J.,* 2014, **244**, 335.

[33] Q. J. Xiang, J. G. Yu and M. Jaroniec, *J. Am. Chem. Soc.,* 2012, **134**, 6575.

[34] J. M. Cai, P. Ruffieux, R. Jaafar, M. Bieri, T. Braun, S. Blankenburg, M. Muoth, A. P. Seitsonen, M. Saleh, X. L.Feng, K. Muellen and R. Fasel, *Nature,* 2010, **466**, 470.

[35] L. Huang, F. Peng, H. Wang, H. Yu and Z. Li, *Cataly. Comm.,* 2009, **10**, 1839.

[36] F. B. Li and X. Z Li, *Chemosphere,* 2002, **48**, 1103.

[37] J. Y. Zhu, Y. Cao and J. H. He, *J. Colloid. Interf. Sci.,* 2014, **420**, 119.

[38] K. K. Manga, S. Wang, M. Jaiswal, Q. Bao and K. P. Loh, *Adv. Mater.,* 2010, **22**, 5265.

[39] G. Eda, C. Mattevi, H. Yamaguchi, H. Kim and M. Chhowalla, *J. Phys. Chem. C,* 2009, **113**,15768.

[40] M. Yang, J. Xu, J. Wei, J. L. Sun, W. Liu and J. L. Zhu, *Appl. Phys. Lett.,* 2012, **100**, 53113.

[41] X. Bai, X. Y. Zhang, Z. L. Hua, W. Q. Ma, Z. Y. Dai, X. Huang and H. X. Gu, *J. Alloy. Comp.,* 2014, **599**, 10.

[42] S. Stankovich, D. A. Dikin and R. D. Piner, *Carbon,* 2007, **45**, 1558.

Fig. captions.

Fig. 1 XRD patterns (a); SEM image (b) and FTIR spectra (c) of the as-prepared RGO/P25 composites with various RGO contents

Fig. 2 (a) Raman map; (b) Raman spectrum; (c) Raman mapping image of TiO_2 ($E_{g(1)}$ mode)

and (d) Raman mapping image of RGO (2D mode) for the 0.75 wt% RGO/P25 composite

Fig. 3 UV-Vis spectra of the as-prepared RGO/P25 composites with various RGO contents

Fig. 4 Photodegradation curves of P25 and various RGO/P25 composites: (a) under UV light irradiation; (b) under visible light irradiation

Fig. 5 Schematic illustration of the photocatalytic process in the RGO/P25 composites

(a)

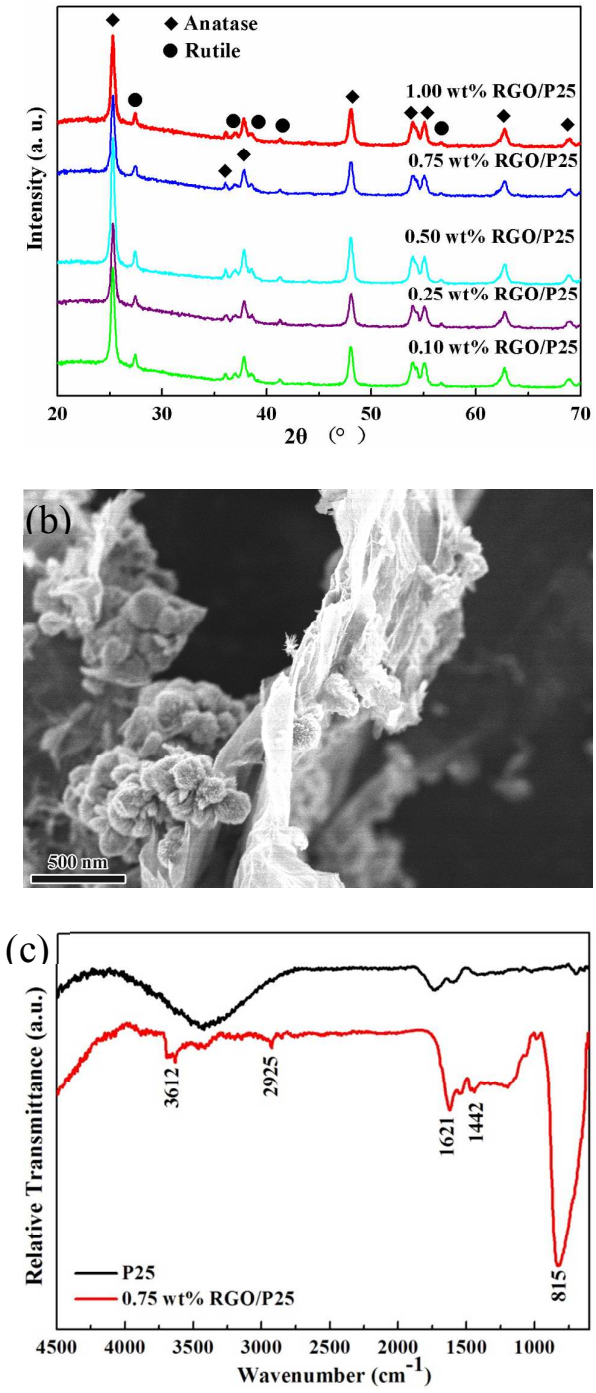

Fig. 1 XRD patterns (a); SEM image (b) and FTIR spectra (c) of the as-prepared RGO/P25 composites with various RGO contents

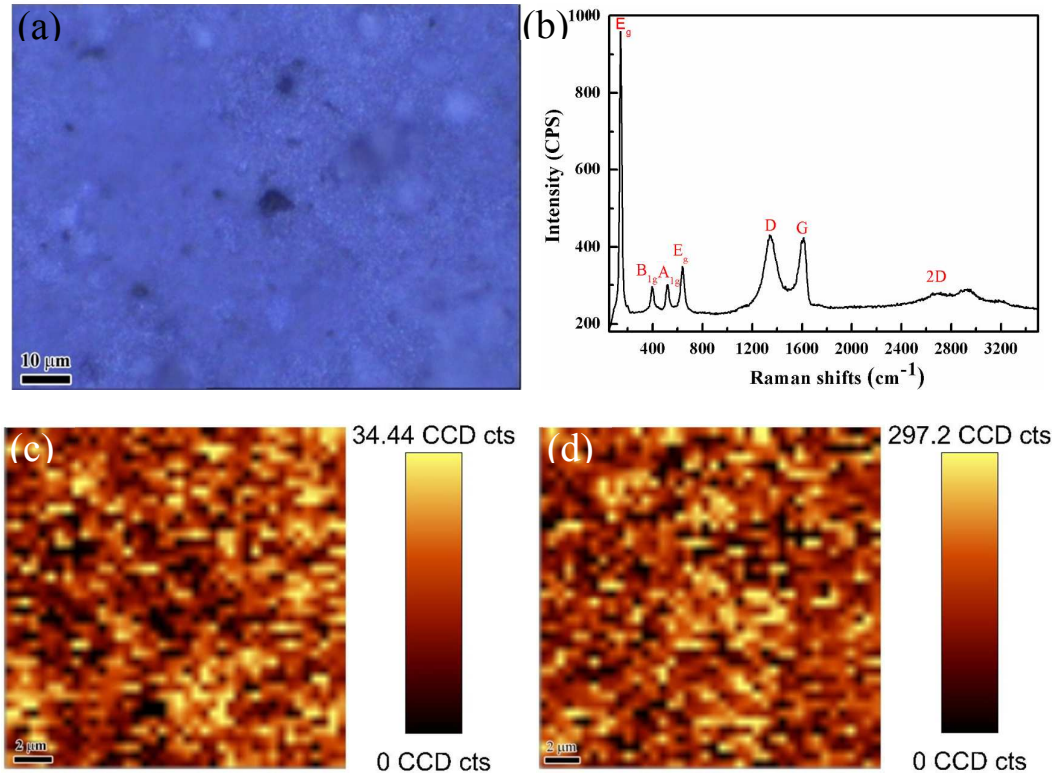

Fig. 2 (a) Raman map; (b) Raman spectrum; (c) Raman mapping image of TiO_2 ($E_{g(1)}$ mode) and (d) Raman mapping image of RGO (2D mode) for the 0.75 wt% RGO/P25 composite

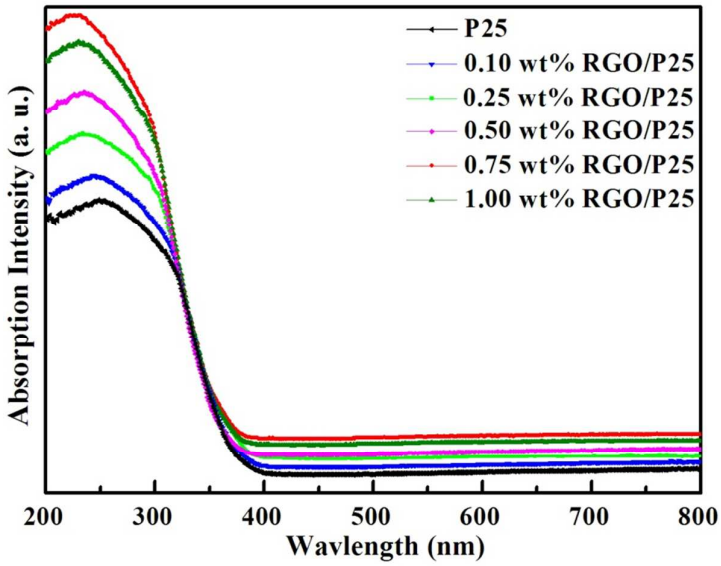

Fig. 3 UV-Vis spectra of the as-prepared RGO/P25 composites with various RGO contents

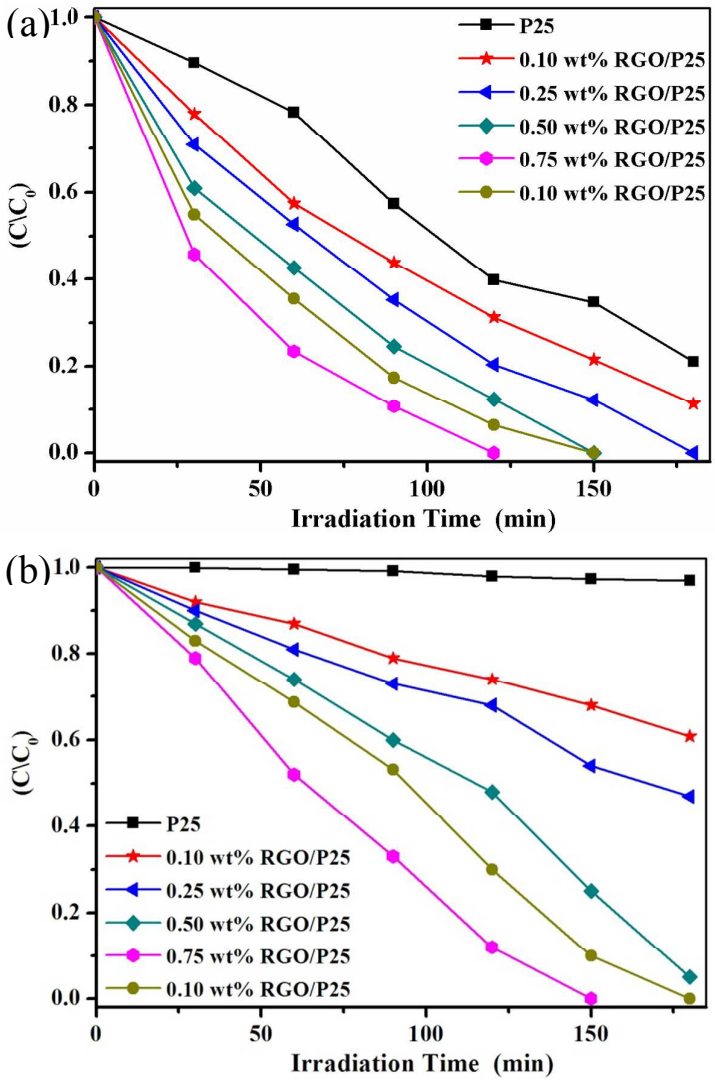

Fig. 4 Photodegradation curves of P25 and various RGO/P25 composites: (a) under UV light irradiation; (b) under visible light irradiation

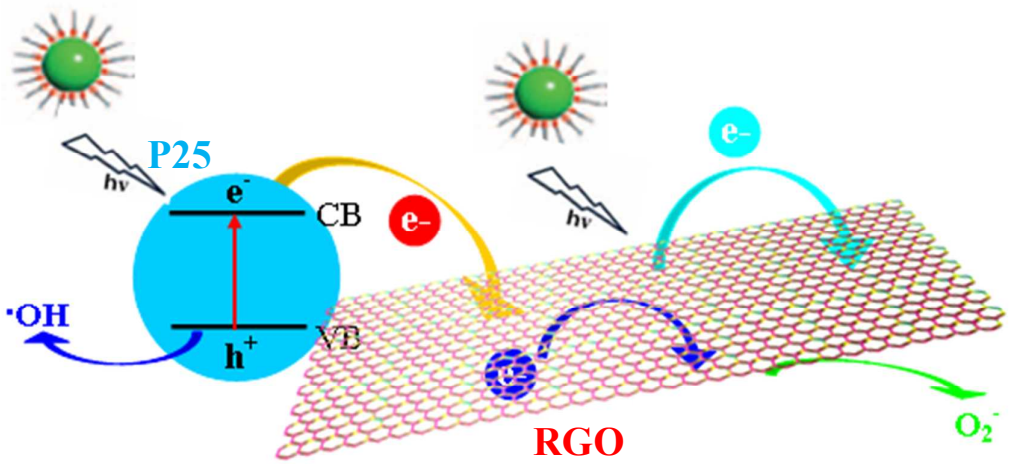

Fig. 5 Schematic illustration of the photocatalytic process in the RGO/P25 composites

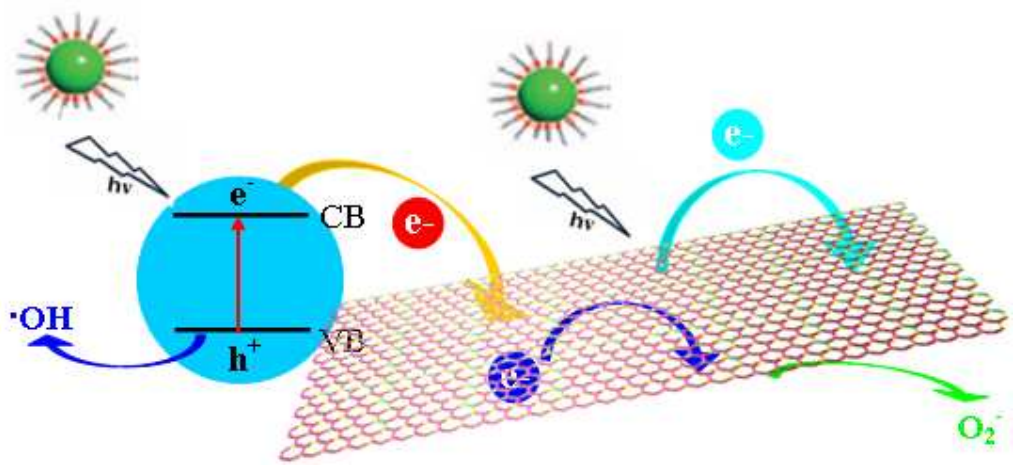

0.75 wt% RGO/P25 composite possesses the photodegradation rate of 100% after 120 and 150 minutes' irradiation under the UV and visible light irradiation